

Exotic low-energy excitations emergent in the random Kitaev magnet Cu_2IrO_3

Y. S. Choi,¹ C. H. Lee,¹ S. Lee,¹ Sungwon Yoon,¹ W.-J. Lee,¹ J. Park,¹ Anzar Ali,² Yogesh Singh,² Jean-Christophe Orain,³ Gareoung Kim,⁴ Jong-Soo Rhyee,⁴ Wei-Tin Chen,⁵ Fangcheng Chou,^{5,6,7} and Kwang-Yong Choi^{1,*}

¹*Department of Physics, Chung-Ang University, Seoul 06974, Republic of Korea*

²*Department of Physical Sciences, Indian Institute of Science Education and Research Mohali, Sector 81, S. A. S. Nagar, Manauli 140306, India*

³*Laboratory for Muon Spin Spectroscopy, Paul Scherrer Institute, 5232 Villigen PSI, Switzerland*

⁴*Department of Applied Physics, Kyung Hee University, Yongin 17104, Republic of Korea*

⁵*Center for Condensed Matter Sciences, National Taiwan University, Taipei 10617, Taiwan*

⁶*National Synchrotron Radiation Research Center, Hsinchu 30076, Taiwan*

⁷*Taiwan Consortium of Emergent Crystalline Materials, Ministry of Science and Technology, Taipei 10622, Taiwan*

We report on magnetization $M(H)$, dc/ac magnetic susceptibility $\chi(T)$, specific heat $C_m(T)$ and muon spin relaxation (μSR) measurements of the Kitaev honeycomb iridate Cu_2IrO_2 with quenched disorder. In spite of the chemical disorders, we find no indication of spin glass down to 260 mK from the $C_m(T)$ and μSR data. Furthermore, a persistent spin dynamics observed by the zero-field muon spin relaxation evidences an absence of static magnetism. The remarkable observation is a scaling relation of $\chi[H, T]$ and $M[H, T]$ in H/T with the scaling exponent $\alpha = 0.26 - 0.28$, expected from bond randomness. However, $C_m[H, T]/T$ disobeys the predicted universal scaling law, pointing towards the presence of low-lying excitations in addition to random singlets. Our results signify an intriguing role of quenched disorder in a Kitaev spin system in creating low-energy excitations possibly pertaining to Z_2 fluxes.

The exactly solvable Kitaev honeycomb model provides a novel route to achieve elusive topological and quantum spin liquids [1, 2]. Exchange frustration of bond-dependent Ising interactions fractionalizes the $j_{\text{eff}} = \frac{1}{2}$ spin into itinerant Majorana fermion and static Z_2 gauge flux [3–5]. Edge-sharing of octahedrally coordinated metal ions subject to strong spin-orbit coupling supports the realization of Kitaev-type interactions [6–8].

In the quest for a Kitaev honeycomb magnet, the family of A_2IrO_3 ($\text{A} = \text{Na}, \text{Li}$) and $\alpha\text{-RuCl}_3$ are considered prime candidate materials [9–16]. In these compounds, however, the theoretically predicted spin-liquid state is preempted by long-range magnetic order due to structural imperfections. As the real materials are vulnerable to a monoclinic stacking of honeycomb layers, non-Kitaev terms seem inevitable. A related issue is to engineer local crystal environments towards an optimal geometry to maximize the Kitaev interactions.

Very recently, the new Kitaev honeycomb iridates $\text{H}_3\text{LiIr}_2\text{O}_6$ and Cu_2IrO_3 have been derived from their ancestors A_2IrO_3 through soft structural modifications [17, 18]. $\text{H}_3\text{LiIr}_2\text{O}_6$ is obtained by replacing the interlayer Li^+ ions with H^+ from $\alpha\text{-Li}_2\text{IrO}_3$, while the honeycomb layer remains intact. A scaling of the specific heat and NMR relaxation rate gives evidence for the presence of fermionic excitations [17]. In stabilizing a Kitaev-like spin liquid, hydrogen disorders turn out to a key ingredient by enhancing Kitaev exchange interactions and promoting spin disordering [19, 20]. In case of Cu_2IrO_3 , all of the A-site cations of Na_2IrO_3 are permuted by Cu^+ ions. Consequently, in-plane bond disorders become significant in determining magnetic behavior.

Figure 1(a) presents the crystal structure of Cu_2IrO_3

(isostructural to Na_2IrO_3 with $C2/c$ space group), in which the honeycomb layers are stacked by CuO_2 dumbbells, distinct from CuO_6 octahedra within the honeycomb layers. The interlayer dumbbell structure arises from the eclipsed stacking of adjacent layers that align the oxygen and interlayer copper atoms in a line. We note that the CuO_2 dumbbells in Cu_2IrO_3 and the linear O-H-O links in $\text{H}_3\text{LiIr}_2\text{O}_6$ have structural similarities in bridging the stacking of honeycomb layers. This structural alteration leads to an elongation of the c -axis and closeness of the Ir-Ir-Ir bond angles to the ideal 120° , compared to its predecessor Na_2IrO_3 [see Fig. 1(b)]. However, little is known about its underlying magnetism.

In this paper, we provide thermodynamic and μSR spectroscopic signatures of a proximate spin-liquid state. We find a scaling relation of the (T, H) -dependent magnetization and ac susceptibility in T/H , but not of the (T, H) -dependent specific heat. This observation suggests the presence of emergent low-lying excitations in addition to the random singlets expected from bond disorders.

Polycrystalline samples of Cu_2IrO_3 were prepared by a topotactic reaction as described in Ref. [18]. Dc and ac magnetic susceptibilities were measured using a SQUID and a vibrating sample magnetometer (Quantum Design MPMS and VSM). The magnetization measurements up to 14 T were carried out using a Physical Property Measurement System (Quantum Design PPMS Dynacool). Specific heat was measured with the thermal-relaxation method using an option of the PPMS apparatus with a ^3He insert. High-field magnetization curves were recorded with a nondestructive pulsed magnet at the Dresden High Magnetic Field Laboratory. Zero-field

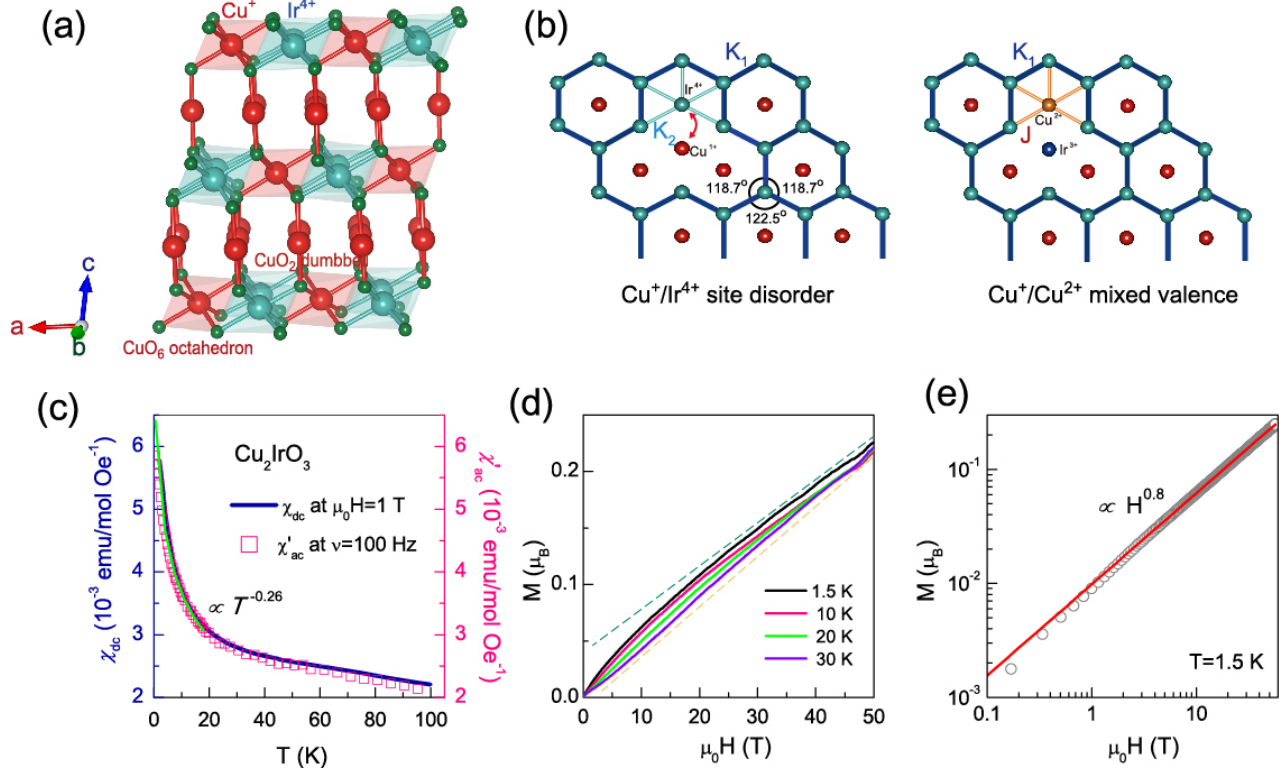


FIG. 1. (a) Crystal structure of Cu_2IrO_3 consisting of edge-sharing $(\text{Ir}_{2/3}\text{Cu}_{1/3})\text{O}_6$ octahedra in the honeycomb layers and linear CuO_2 dumbbells between the layers. The greenish blue, red, and green spheres represent Ir, Cu and O ions, respectively. (b) Sketch of two types of chemical disorders occurring in the honeycomb plane. $\text{Cu}^{1+}/\text{Ir}^{4+}$ cation disorders and $\text{Cu}^{1+}(\text{Ir}^{4+})/\text{Cu}^{2+}(\text{Ir}^{3+})$ mixed valence not only create nonmagnetic impurities but also supply a new triangular motif. (c) Comparison of the dc and ac magnetic susceptibility of Cu_2IrO_3 measured with an applied field of 1 T and at $\nu = 100$ Hz and $H_{\text{osc}} = 10$ Oe, respectively. The green solid line is a fit to a power-law $\chi(T) \sim T^{-\alpha_s}$ with $\alpha_s = 0.26$. (d) High-field magnetization curves $M(H)$ measured at $T = 1.5, 10, 20,$ and 30 K. (e) Log-log plot of $M(H)$ at $T = 1.5$ K. The solid red line is a power-law fit $M(H) \sim H^{1-\alpha_m}$ with $\alpha_m \approx 0.2$.

(ZF)- and longitudinal-field (LF)- μSR experiments were performed with the DOLLY spectrometer at PSI (Villigen, Switzerland). For measurements down to 0.26 K, the samples were loaded into the Variox cryostat equipped with Heliox insert. All of the obtained μSR data were analyzed using the software package Musfit [21].

Figure 1(c) shows the T -dependence of the static magnetic susceptibility $\chi_{\text{dc}}(T)$ of Cu_2IrO_3 measured at $\mu_0 H = 1$ T, together with the real component of ac susceptibility $\chi'_{\text{ac}}(T)$. As $T \rightarrow 0$ K, both $\chi_{\text{dc}}(T)$ and $\chi'_{\text{ac}}(T)$ exhibit a steep increase without obvious saturation or kink, in spite of the large Curie-Weiss temperature $\Theta_{\text{CW}} = -110$ K [18]. It is remarkable that both $\chi_{\text{dc}}(T)$ and $\chi'_{\text{ac}}(T)$ are described by a power-law increase $\chi(T) \sim T^{-\alpha_s}$ with $\alpha_s = 0.26$ for temperatures below 20 K. Such a sub-Curie law behavior is indicative of the presence of abundant low-energy excitations. As shown in Fig. 1(d), the high-field magnetization curves $M(H)$ at selected low temperatures display clear deviations from a linear- H dependence. Significantly, we find that the $T = 1.5$ K $M(H)$ follows a power-law de-

pendence $M(H) \sim H^{1-\alpha_m}$ with $\alpha_m = 0.2$ over an entirely measured field range [see a log-log plot of $M(H)$ in Fig. 1(e)]. The commonly observed power-law behavior of $\chi(T)$ and $M(H)$ with $\alpha_s \approx \alpha_m$ constitutes a hallmark of random magnetic interactions [22–24].

Given the sizable $\text{Cu}^{1+}/\text{Ir}^{4+}$ intersite disorder and $\text{Cu}^{1+}/\text{Cu}^{2+}$ mixed valence [18], magnetic ions (either Ir^{4+} or Cu^{2+}) occupy randomly at the center of the honeycomb lattice, while nonmagnetic ions (either Cu^{1+} or Ir^{3+}) go on the vertex of the honeycomb lattice. Based on the power-law dependence of $M(H)$ persisting down to 0.3 T in Fig. 1(e), we conclude that the chemical disorders are mostly confined within the honeycomb layers. As sketched in Fig. 1(b), an impact of the quenched disorders on magnetism is twofold. One is to introduce spin vacancies, and the other is to generate a spin triangular motif which has a different coupling constant from the original honeycomb lattice, thereby creating a random distribution in exchange constants.

An essence of random magnetism consists in low-energy random singlets generated in the matrix of a

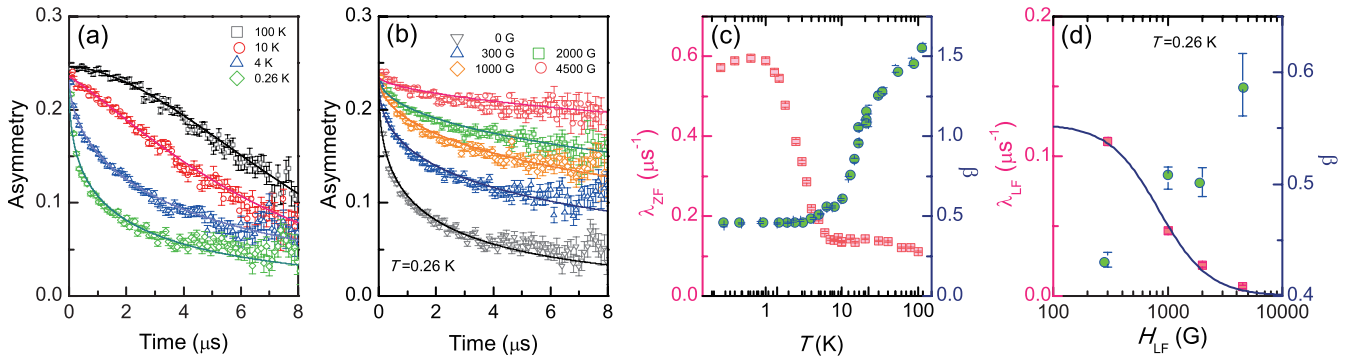


FIG. 2. (a) ZF- μ SR spectra of Cu_2IrO_3 at selected temperatures. (b) Field dependence of LF- μ SR spectra measured at $T = 0.26$ K in an applied field of $H = 0 - 4500$ G. The solid lines are fits to the stretched exponential function. (c) The muon relaxation rate $\lambda_{\text{ZF}}(T)$ and the stretch exponent $\beta(T)$ extracted from fitting to the ZF data. (d) Longitudinal-field dependence of the muon relaxation rate $\lambda_{\text{LF}}(H_{\text{LF}})$ and the stretch exponent $\beta(H_{\text{LF}})$ extracted from the $T = 0.26$ K LF data. The solid curve denotes the fit of $\lambda_{\text{LF}}(H_{\text{LF}})$ to the Redfield formula.

quantum disordered state, which give rise to a diverging low-energy excitation [22, 23]. Before proceeding, we first clarify whether the quenched disorder induces frozen moments. For this purpose, we employ a μ SR technique, allowing differentiating a quantum disordered from a weakly ordered state.

Figures 2(a) and 2(b) show the ZF- μ SR spectra at selected temperatures and the LF- μ SR spectra measured at $T = 0.26$ K in an applied field of $H = 0 - 4500$ G. The μ SR data at all temperatures and fields are successfully described by the stretched-exponential function $P_{\text{ZF}}(t) = P_0 \exp[-(\lambda_{\text{ZF}}t)^\beta] + P_{\text{bg}}$, where λ_{ZF} is the muon relaxation rate and β is the stretching exponent. The T -independent P_{bg} term represents a background contribution, which originates from muons implanted in the silver sample holder or the cryostat.

With decreasing temperature, the ZF- μ SR spectra gradually change their asymmetry lineshape from a Gaussian- to a Lorentzian-like relaxation form. At the measured lowest temperature of 0.26 K, we observe neither spontaneously oscillating component nor missing initial $P_{\text{ZF}}(t)$. Rather, the low- T ZF- μ SR data display a dynamic relaxation with no indication to a recovery of a one-third tail at long times. The temperature evolution of a relaxation lineshape excludes any local static fields at the muon stopping site. Also, the LF dependence of the μ SR spectra supports that the Ir moments remain in a dynamically fluctuating state at least down to $T = 0.26$ K. As plotted in Fig. 2(b), even applying the longitudinal field of $H_{\text{LF}} = 4500$ G, there is a substantially decoupled relaxation. If the low- T muon spin relaxation at zero field arises from static magnetism, the local static field is estimated to be $B_{\text{loc}} \approx 4.4$ G. In this case, one would observe a full polarization of the μ SR spectra upon the application of about 50 G longitudinal fields.

We next turn to the T and H evolution of the ob-

tained fit parameters. As seen from Fig. 2(c), with decreasing temperature $\lambda_{\text{ZF}}(T)$ starts to increase at 6 K and then saturates at about 1 K. Such a low- T plateau in $\lambda_{\text{ZF}}(T)$, representing a persistent spin dynamics, has been observed in a range of geometrically frustrated magnets having spin freezing or weak magnetic order, let alone quantum spin liquids [25–28]. In parallel to $\lambda_{\text{ZF}}(T)$, the stretching exponent decreases rapidly from $\beta > 1$ to $\beta < 1$ on cooling through 10 K, and then levels off to $\beta \approx 0.5$ below 2 K. The obtained value of β at the base temperature is larger than $\beta = 1/3$ (value of canonical spin glass).

Shown in Fig. 2(d) is the LF-dependence of $\lambda_{\text{LF}}(H_{\text{LF}})$ and $\beta(H_{\text{LF}})$ measured at $T = 0.26$ K. In the Redfield model, $\lambda_{\text{LF}}(T)$ is associated with the fluctuation frequency ν and the fluctuating time-averaged local field $\langle H_{\text{loc}}^2 \rangle$ by $\lambda_{\text{LF}}(H_{\text{LF}}) = 2\gamma_\mu^2 \langle H_{\text{loc}}^2 \rangle \nu / (\nu^2 + \gamma_\mu^2 H_{\text{LF}}^2)$ [29, 30]. Here, γ_μ is the muon gyromagnetic ratio. From fits of the $T = 260$ mK data, we obtain $\nu \sim 72$ MHz and $H_{\text{loc}} \sim 25$ G. The determined ν (H_{loc}) is roughly two times slower (larger) than $\nu \sim 150$ MHz and $H_{\text{loc}} \sim 18$ G of the well-investigated spin-liquid material $\text{ZnCu}_3(\text{OH})_6\text{Cl}_2$ [26]. On the LF application, $\beta(H_{\text{LF}})$ steadily increases, implying the gradual quenching of widely distributed fluctuating local fields. Taken the μ SR data together, we conclude that Cu_2IrO_3 features a dynamically fluctuating state. Based on the relatively small value of $\beta \approx 0.5$, however, we cannot totally exclude some tendency to weak spin freezing, if any.

In the followings, we will discuss an intricate relation between quenched disorder and critical spin correlations.

In Fig. 3(a), the H and T dependences of χ'_{ac} are plotted on the log-log scale in the applied fields of $\mu_0 H = 0 - 3$ T. With increasing field, $\chi'_{\text{ac}}(T)$ is systematically reduced, yet still maintains a power-law dependence, while changing the exponent from $\alpha_s = 0.26$ at 0 T to 0.13 to 3 T. In an attempt to corroborate dynamic

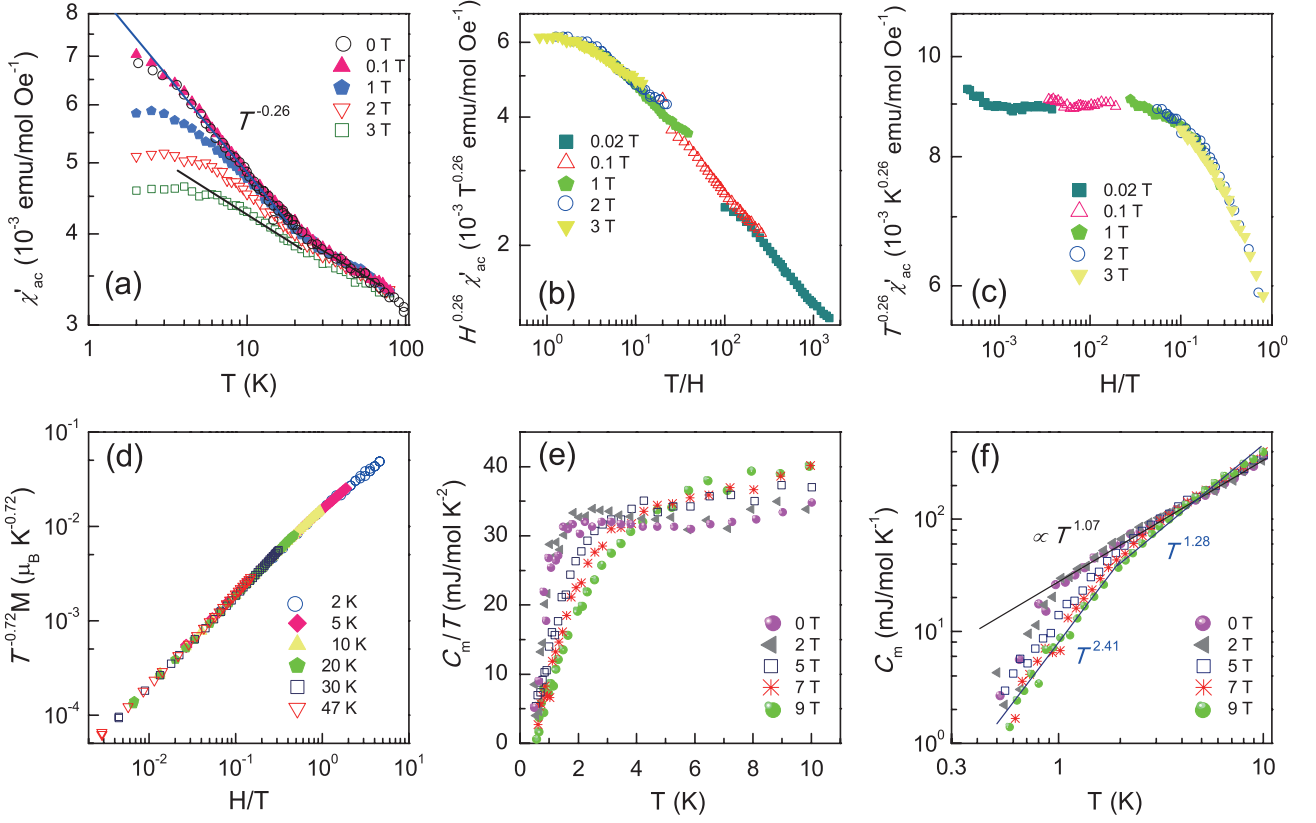


FIG. 3. (a) The real component of the ac susceptibility $\chi'_{ac}(T)$ plotted against temperature for Cu_2IrO_3 under various external fields. The solid line is a power-law dependence of the 0 T data, $\chi'_{ac}(T) \sim T^{-0.26}$. (b) Log-log scaled plot of $H^{0.26}\chi'_{ac}$ vs T/H displays a scaling relation. (c) $T^{0.26}\chi'_{ac}$ shows a scaling with H/T . (d) $T - H$ scaling of $M(H)$ plotted on a log-log scale. (e) Magnetic specific heat divided by temperature C_m/T versus T for various magnetic fields. (f) Log-log plot of the same (T, H) -dependent C_m . The solid lines are the fits of the C_m data to a power law.

scaling behavior, we plot $H^{\alpha_s}\chi'_{ac}$ vs T/H and $T^{\alpha_s}\chi'_{ac}$ vs H/T in Figs. 3(b) and 3(c), respectively. Strikingly, the (H, T) -dependent χ'_{ac} data overlap over three orders of magnitude with the same value of $\alpha_s = 0.26$. We provide further supportive evidence for universal scaling behavior from testing the similar scaling behavior in the $M(H)$ data measured up to $\mu_0 H = 14$ T at various temperatures (2, 5, 10, 20, 30, and 47 K). We plot MT^{α_m-1} against H/T in Fig. 3(d), and obtain the exponent value of $\alpha_m = 0.28$ that guarantees a sufficient data collapse onto a single scaling curve. Within the error bars, the scaling exponent of $0.26 - 0.28$ agrees exceptionally well between the two distinct thermodynamic quantities. This is reminiscent of universal scaling observed in a certain class of frustrated quantum magnets $\text{H}_3\text{LiIr}_2\text{O}_6$, $\text{LiZn}_2\text{Mo}_3\text{O}_8$, and $\text{ZnCu}_3(\text{OH})_6\text{Cl}_2$, which commonly share proximate spin liquids and quenched disorder [24].

We further explore the specific heat scaling. Figure 3(e) shows a C_m/T versus T plot at low temperatures of $T = 0.5 - 10$ K under the external magnetic fields of $\mu_0 H = 0 - 9$ T. The zero-field C_m/T data shows little variation with temperature down to 2 K and then

a rapid drop below 1 K. With increasing magnetic field, the C_m/T contribution below 4 K is steadily suppressed. Unlike the afore-mentioned quantum disordered magnets with quenched disorder, the zero-field C_m/T data lacks any upturn at extremely low temperatures [24]. In addition, we could find no scaling and data collapse of $C_m[T, H]/T$ in T/H (not shown here).

To figure out the failure of the predicted power-law scaling within a random magnetism scenario, we replot C_m vs T on a log-log scale in Fig. 3(f). The magnetic specific heat is described by $C_m(T) \sim T^\gamma$. Obviously, the exponent of $\gamma \approx 1.07$ at $\mu_0 H = 0$ T defies the $T^{1-\alpha}$ scaling ($\alpha = 0.26 - 0.28$) obtained from $M(H)$ and χ'_{ac} . Rather, a nearly T -linear contribution is reminiscent of gapless spinon excitations reported in the spin-liquid candidate materials [31]. Furthermore, the low- T and high- H C_m data display a $T^{2.41}$ dependence, stronger than the T^2 dependence often reported in the frustrated magnets with the weak bond disorder, obeying the power-law scaling law [24]. Admittedly, there is some uncertainty in evaluating the lattice contribution. As the $\chi'[T, H]$ and $M[T, H]$ scalings are limited above 2 K, however, the specific heat anomaly may be resolved by invoking

the chemical disorder that alters extremely low-energy excitations pertaining to Z_2 fluxes.

To conclude, we combine μ SR with thermodynamic measurements to unravel a ground state and bond-randomness-induced scalings in the random Kitaev magnet Cu_2IrO_2 .

The ZF- and LF- μ SR data evidence the formation of a spin-liquid-like ground state, in which the spins remain almost dynamic down to 260 mK. This sets up a setting for the random singlet model on the background of a quantum disordered state. As anticipated, both magnetization and ac magnetic susceptibility obey a temperature-field scaling. Thus, Cu_2IrO_2 seems to belong to a class of frustrated quantum magnets that are proximate to a quantum disordered state and are subject to quenched disorder. However, the purported random singlet scenario is not compatible with a lacking scaling in the magnetic specific heat. This highlights an intriguing character of chemical disorders, which generates not only random exchange interactions but also spin vacancies [see Fig. 1(b)]. Noteworthy is that the magnetic specific heat shows a nearly T -linear relationship at low temperatures of $T = 1 - 10$ K, typical for gapless excitations, and then a strong T -dependence below 1 K, indicative of the development of gapful excitations at extremely low temperatures.

Recent theoretical calculations show that vison and Majorana zero mode can be created in the vicinity of a site vacancy [32]. These zero-energy resonances are largely hidden to static spin susceptibility and, thus, may provide a possible account of the specific heat anomaly. Ultralow-temperature experiments and future theoretical studies are requested to clarify whether this scenario is applicable to Cu_2IrO_2 .

Note added.- During writing the manuscript, we noted that a related study by E. M. Kenney *et al.* was posted in preprint [33], which observed a coexistence of static and dynamic magnetism. Unlike their μ SR data, the absence of frozen magnetic moments is clear in our sample, thereby ruling out a nucleation of the quenched disorder. As to the dynamic magnetism, our data are consistent with their results.

ACKNOWLEDGMENTS

This work was supported by Korea Research Foundation (KRF) Grants (No. 2018-0189 and No. 2018-0099) funded by the Korea government (MEST). We acknowledge the support of the HLD at HZDR, member of the European Magnetic Field Laboratory (EMFL).

* kchoi@cau.ac.kr

- [1] A. Kitaev, *Annals of Phys.* **321**, 2 (2006).
- [2] G. Baskaran, S. Mandal and R. Shankar, *Phys. Rev. Lett.* **98**, 247201 (2007).
- [3] J. Knolle, D. L. Kovrizhin, J. T. Chalker, and R. Moessner, *Phys. Rev. Lett.* **112**, 207203 (2013).
- [4] J. Knolle, G.-W. Chern, D. L. Kovrizhin, R. Moessner, and N. B. Perkins, *Phys. Rev. Lett.* **113**, 187201 (2014).
- [5] J. Nasu, M. Udagawa, and Y. Motome, *Phys. Rev. Lett.* **113**, 197205 (2014).
- [6] G. Jackeli and G. Khaliullin, *Phys. Rev. Lett.* **102**, 017205 (2009).
- [7] J. Chaloupka, G. Jackeli and G. Khaliullin, *Phys. Rev. Lett.* **105**, 027204 (2010).
- [8] J. G. Rau, E. K.-H. Lee, and H.-Y. Kee, *Phys. Rev. Lett.* **112**, 077204 (2014).
- [9] Y. Singh and P. Gegenwart, *Phys. Rev. B* **82**, 064412 (2010).
- [10] S. K. Choi, R. Coldea, A. N. Kolmogorov, T. Lancaster, I. I. Mazin, S. J. Blundell, P. G. Radaelli, Y. Singh, P. Gegenwart, K. R. Choi, S.-W. Cheong, P. J. Baker, C. Stock, and J. Taylor, *Phys. Rev. Lett.* **108**, 127204 (2012).
- [11] T. Takayama, A. Kato, R. Dinnebier, J. Nuss, H. Kono, L. S. I. Veiga, G. Fabbri, D. Haskel, and H. Takagi, *Phys. Rev. Lett.* **114**, 077202 (2015).
- [12] K. A. Modic, T. E. Smidt, I. Kimchi, N. P. Breznay, A. Biffin, S. K. Choi, R. D. Johnson, R. Coldea, P. Watkins-Curry, G. T. McCandless, J. Y. Chan, F. Gandara, Z. Islam, A. Vishwanath, A. Shekhter, R. D. McDonald, and J. G. Analytis, *Nat. Commun.* **5**, 4203 (2014).
- [13] A. Glamazda, P. Lemmens, S.-H. Do, Y. S. Choi, and K.-Y. Choi, *Nat. Commun.* **7**, 12286 (2016).
- [14] K. W. Plumb, J. P. Clancy, L. J. Sandilands, V. Vijay Shankar, Y. F. Hu, K. S. Burch, Hae-Young Kee, and Young-June Kim, *Phys. Rev. B* **90**, 041112(R) (2014).
- [15] A. Banerjee, C. A. Bridges, J.-Q. Yan, A. A. Aczel, L. Li, M. B. Stone, G. E. Granroth, M. D. Lumsden, Y. Yiu, J. Knolle, S. Bhattacharjee, D. L. Kovrizhin, R. Moessner, D. A. Tennant, D. G. Mandrus, and S. E. Nagler, *Nat. Mater.* **15**, 733 (2016).
- [16] S.-H. Do, S.-Y. Park, J. Yoshitake, J. Nasu, Y. Motome, Y. S. Kwon, D. T. Adroja, D. J. Voneshen, Kyoo Kim, T.-H. Jang, J.-H. Park, K.-Y. Choi, and S. Ji, *Nat. Phys.* **13**, 1079 (2017).
- [17] K. Kitagawa, T. Takayama, Y. Matsumoto, A. Kato, R. Takano, Y. Kishimoto, S. Bette, R. Dinnebier, G. Jackeli, and H. Takagi, *Nature* **554**, 341 (2018).
- [18] M. Abramchuk, C. Ozsoy-Keskinbora, J. W. Krizan, K. R. Metz, D. C. Bell, and F. Tafti, *J. Am. Chem. Soc.* **139**, 15371 (2017).
- [19] K. Slagle, W. Choi, L. E. Chern, and Y. B. Kim, *Phys. Rev. B* **97**, 115159 (2018).
- [20] R. Yadav, R. Ray, M. S. Eldeeb, S. Nishimoto, L. Hozoi, and J. van den Brink *Phys. Rev. Lett.* **121**, 197203 (2018).
- [21] A. Suter, and B.M. Wojek, *Physics Procedia* **30**, 69 (2012).
- [22] S.-k. Ma, C. Dasgupta, and C.-k. Hu, *Phys. Rev. Lett.* **43**, 1434 (1979).
- [23] J. E. Hirsch and J. V. Jose, *Phys. Rev. B* **22**, 5339 (1990).
- [24] I. Kimchi, J. P. Sheckelton, T. M. McQueen, and P. A. Lee *Nat. Commun.* **9**, 4367 (2018).
- [25] J. S. Gardner, S. R. Dunsiger, B. D. Gaulin, M. J. P. Gingras, J. E. Greedan, R. F. Kiefl, M. D. Lumsden, W.

- A. MacFarlane, N. P. Raju, J. E. Sonier, I. Swainson, and Z. Tun, Phys. Rev. Lett. **82**, 1012 (1999).
- [26] P. Mendels, F. Bert, M. A. de Vries, A. Olariu, A. Harrison, F. Duc, J. C. Trombe, J. S. Lord, A. Amato, and C. Baines, Phys. Rev. Lett. **98**, 077204 (2007).
- [27] Y. Li, D. Adroja, P. K. Biswas, P. J. Baker, Q. Zhang, J. Liu, A. A. Tsirlin, P. Gegenwart, and Q. Zhang, Phys. Rev. Lett. **117**, 097201 (2016).
- [28] A. Yaouanc, P. Dalmas de Rotier, A. Bertin, C. Marin, E. Lhotel, A. Amato, and C. Baines, Phys. Rev. B **91**, 104427 (2015).
- [29] A. G. Redfield, IBM J. Research and Development **1**, 19 (1957).
- [30] A. Yaouanc and P. Dalmas de Rotier, *Muon spin rotation, relaxation, and resonance: applications to condensed matter*, Oxford University Press, (2011).
- [31] W.-J. Lee, S.-H. Do, Sungwon Yoon, S. Lee, Y. S. Choi, D. J. Jang, M. Brando, M. Lee, E. S. Choi, S. Ji, Z. H. Jang, B. J. Suh, and K.-Y. Choi, Phys. Rev. B **96**, 014432 (2017).
- [32] M. Udagawa arXiv:1811.02092 (2018).
- [33] E. M. Kenney, C. U. Segre, W. Lafargue-Dit-Hauret, O. I. Lebedev, M. Abramchuk, A. Berlie, S. P. Cottrell, G. Simutis, F. Bahrami, N. E. Mordvinova, J. L. McChesney, G. Fabbri, D. Haskel, X. Rocquefelte, M. J. Graf, and F. Tafti, arXiv:1811.00565 (2018).